General Disclaimer

One or more of the Following Statements may affect this Document

- This document has been reproduced from the best copy furnished by the organizational source. It is being released in the interest of making available as much information as possible.

- This document may contain data, which exceeds the sheet parameters. It was furnished in this condition by the organizational source and is the best copy available.

- This document may contain tone-on-tone or color graphs, charts and/or pictures, which have been reproduced in black and white.

- This document is paginated as submitted by the original source.

- Portions of this document are not fully legible due to the historical nature of some of the material. However, it is the best reproduction available from the original submission.

Produced by the NASA Center for Aerospace Information (CASI)

(NASA-TM-78855) DIAGNOSTIC EVALUATIONS OF A BEAM-SHIELDED 8-cm MERCURY ION THRUSTER (NASA) 25 p HC A02/MF A01 CSCL 21C

N78-21207

Unclas
G3/20 12416

NASA TECHNICAL MEMORANDUM

NASA TM-78855

NASA TM-78855

DIAGNOSTIC EVALUATIONS OF A BEAM-SHIELDED 8-CM MERCURY ION THRUSTER

by S. Nakanishi
Lewis Research Center
Cleveland, Ohio 44135

TECHNICAL PAPER to be presented at the
Thirteenth International Electric Propulsion Conference
cosponsored by the American Institute of Aeronautics and Astronautics
and the Deutsche Gesselschaft fur Luft-und Raumfahrt
San Diego, California, April 25-27, 1978

MAY 1978

DIAGNOSTIC EVALUATIONS OF A BEAM-SHIELDED 8-CM MERCURY ION THRUSTER

by S. Nakanishi

National Aeronautics and Space Administration
Lewis Research Center
Cleveland, Ohio 44135

E-9581

ABSTRACT

An engineering model thruster fitted with a remotely actuated graphite fiber polyimide composite beam shield was tested in a 3- by 6.5-meter vacuum facility for in-situ assessment of beam shield effects on thruster performance. Accelerator drain current neutralizer floating potential and ion beam floating potential increased slightly when the shield was moved into position. A target exposed to the low density regions of the ion beam was used to map the boundaries of energetic fringe ions capable of sputtering. The particle efflux was evaluated by measurement of film deposits on cold, heated, bare, and enclosed glass slides.

INTRODUCTION

High specific impulse mercury ion thrusters have long been considered for application to various spacecraft. A recent study (refs. 1 and 2) of ion thruster application to a 1000-kg geosynchronous communication satellite showed net payload savings of up to 88 kg with a thrust subsystem reliability of 0.948. For 5.1 mN (1.1 mlb) thrust level ion thrusters, other applications, such as a high-performance propulsion module for orbit maneuvers and drag makeup of subsynchronous orbiting spacecraft, have also been identified (ref. 1). The study included experimental evaluation of thruster efflux and interface requirements and discussed techniques to allow the integration of ion thrusters with spacecraft.

A joint Air Force-NASA flight experiment is scheduled for 1981 (ref. 3). In this flight, two complete thrust subsystems, and several diagnostic instruments, will be mounted on a spacecraft carrying two other major experiments with stringent contamination requirements.

To support this flight experiment and provide a technology base for ground/space data correlation, an on-going series of tests are being conducted at the

Star Category 20

NASA Lewis Research Center with a beam-shielded engineering model (EM) 8-cm thruster powered by laboratory supplies. This report presents preliminary results of these tests.

Tests have been performed to determine any effects of the beam shield on thruster performance and to evaluate the characteristics and potential impact of thruster efflux upon spacecraft systems. The data presented herein include current and potential measurements in the ion beam, the sputter erosion pattern due to energetic beam ions, and deposition effects of thruster efflux. Determination of thruster efflux in ground tests is inevitably affected by test facility effects. The results, however, are inclined to be worst case results and viewed as such should add credence and confidence to flight experimental data.

APPARATUS AND PROCEDURE

8-Cm Engineering Model Thruster (EMT)

A photograph of the 8-cm EMT, including the gimbal mount and beam shield, is shown in figure 1. Details of the thruster system are described in references 4 and 5. Design features of specific interest to the present investigation include the Small Hole Accelerator Grid (SHAG) ion optics (compensated), and the graphite fiber-polyimide composite beam shield. For this program, the beam shield was mounted on a remotely actuated hinge to permit movement in and out of position while the thruster was running. The entire beam shield assembly was electrically isolated from the thruster to allow floated or biased operation. Typical performance characteristics of the 8-cm EMT and their variations among three production modules are documented and reported in references 5 and 6.

Test Installation and Facility

A view of the 8-cm EMT mounted on the end cap of the 3- by 6.5-meter vacuum facility is shown in figure 2. The thruster axis was 9 cm below the facility centerline and the accelerator grid projected 55.6 cm into the cylindrical portion of the test chamber. The thruster was thus aligned conveniently relative to existing access ports through which probes and efflux deposition samples were inserted and retracted.

The vacuum facility was equipped with six 81-cm diameter oil diffusion pumps and associated mechanical pumps. A liquid nitrogen cooled cryowall extended over the full length of the vacuum facility and a similarly cooled target was located 4 meters downstream of the accelerator grid plane. Tank pressure with the thruster operating at rated conditions was between 1.5 and 2.5×10^{-7} torr.

Beam Diagnostics and Instrumentation

A schematic layout of the various thruster efflux diagnostic equipment and instrumentation is shown in figure 3. Only selected instrumentation was used in any given test in order to avoid mutual contamination, interference, or shadowing.

The 0.64 cm diameter molybdenum planar probe was located 38.4 cm downstream of the accelerator grid plane and traversed in a horizontal line perpendicular to the thruster axis.

Deposition plates numbered 1, 2, and 3 were 2- by 2- by 0.15-cm thick quartz glass slides enclosed in 2.54- by 2.54- by 1.9-cm deep stainless steel boxes with a 0.64- by 1.27-cm aperture located 1.6 cm from the slide. These samples were mounted on movable rods which permitted the insertion and retraction of samples via vacuum isolation valves during tests.

The arrays of enclosed and unenclosed glass slides were mounted in a horizontal plane at a radius of 50 cm on either side of the thruster axis. The right bank was heated by a swaged coaxial heating element attached along a curved aluminum bracket. The glass slides were held in close contact with the heated bracket and were at approximately its temperature. The left bank was unheated. Both banks carried identical sets of deposition samples located according to the schematic shown in figure 3. The enclosed slides and their enclosures were similar to those described above. These slides are identified by the single digit numbers in the E (for east and W (for west) banks.

The unenclosed glass slides were 2.54- by 7.6- by 0.1-cm thick and located at the forward ends of the mounting brackets and between the enclosures. These slides are identified by two digit numbers in the E and W banks.

The sputter targets were used at the axial locations indicated in figure 3. All targets were 1.34 meter wide by 1.8 meter long by 0.025 mm (1 mil) thick mylar with 150 Å aluminum coating on one side. The target for each test had a central hole size to form the base of a 29° cone with the apex located at the accelerator grid center. The target thus passed the high density core of the ion beam and intercepted only the lower density fringe ions. To keep the back (nonaluminized) side of the target from collecting backsputtered tank wall material, a second sheet of mylar with a central hole 5 cm larger in diameter was attached but kept isolated from the aluminized coating of the target front. This allowed the measurement of ion current collected by the front face only.

Thruster Power Supplies and Instrumentation

The 8-cm EM thruster was powered by a 60 hz laboratory console of the type described in reference 7. The cathode vaporizer flow was automatically controlled to a set-point voltage difference between the cathode keeper and ion chamber anode.

Neutralizer flow rate was manually controlled by maintaining a constant vaporizer temperature. The mercury flow rate to each vaporizer was measured with a 0.5 mm bore capillary tube flow meter. All thruster variables were held at the nominal EM thruster values specified in reference 5.

The laboratory console panel meters were the primary monitors for each thruster variable. In addition, an eight-channel strip chart recorder was used for continuous recording of selected parameters. The beam shield potential was measured by a digital voltmeter having an input impedance of 10 megohms and isolated from the 115-V ac line by an isolation transformer. Beam shield temperatures at the tip and base were monitored with iron-constantan thermocouples and an isolated two-channel strip chart recorder.

Cathode preheating, startup, and operating procedures were in accordance with those currently established and used for all 8-cm EM thrusters. Special operational or test procedures used in diagnostic evaluations are described in conjunction with the Results and Discussion.

RESULTS AND DISCUSSION

Effects of Beam Shield

The beam shield was found to have only minor impact on thruster operation. As noted in Apparatus and Procedure, the movable beam shield provided in situ evaluation of its effects. A transient recording of six thruster variables on a movement of 1 mm/sec time scale is shown in figure 4. The appropriate scale factors for each channel variable and the point of shield movement are indicated. Figure 4(a) shows the transient from shield-in to shield-out positions. Within 1 second of shield movement, the accelerator drain current decreased 0.015 mA and the neutralizer floating potential became less negative about 1.5 V. All other variables remained constant. The perturbations in the cathode and neutralizer keeper voltages were random shifts in the hollow cathode current-voltage characteristics.

A transient recording of thruster variables during shield-out to shield-in movement is shown in figure 4(b). As expected, the accelerator drain current and neutralizer floating potential returned to their original values. The elapsed time between the two sequences was 9 minutes.

The beam shield was mechanically supported but electrically isolated from the thruster ground screen. The effects of varying the shield potential relative to facility ground are shown in figure 5. In figure 5(a) the net positive ion current collected by the shield was zero at the floating potential of -6.5 V relative to ground. Higher negative bias voltages increased the collected current only slightly

to a saturation value of about 0.5 mA.

Increasing the bias voltage positively above floating potential collected increasingly large electron current at the shield. The voltage current curve had the shape expected from Langmuir probe theory.

As shown in figure 5(b), increasing negative bias had little effect upon the neutralizer potential. Positive bias, however, drove the neutralizer floating potential closer to ground. It should be recalled from the transient recordings of figure 4 that the presence of the beam shield increased the neutralizer floating potential 1.5 V negatively from ground. A positive shield bias thus tended to restore the neutralizer floating potential to a no-shield state.

An examination of shield effects upon the ion exhaust beam was made by obtaining beam profiles with the planar probe biased 15 V negative with respect to ground. The profiles taken normal to the thruster axis in rapid succession with shield-out and shield-in are shown in figure 6. The beam center was taken to be the point at which a clearly defined peak was obtained with the shield in. The probe position indicator reading corresponding to this peak in current was thereafter used as the beam center position. With the shield-in, the beam profile was slightly broadened and the peak current at the center was reduced. The neutralizer, and hence the beam shield, was located to the left of center in figure 6. No obvious assymetry was introduced by the presence of the shield. It should be pointed out that the beam was highly peaked and attenuated to less than 5 percent of peak value at 15 cm radius which corresponds to an angle of about 21.5°. Inasmuch as no range changing was used in the current measurement, resolution was poor at radii beyond 20 cm which corresponds to an angle of 27.5°. A ray drawn at this angle from the accelerator grid center did not intercept the beam shield tip, thus registering no measurable difference in beam profile symmetry.

The floating potential profile across the exhaust beam was obtained by isolating the planar probe with a differential input amplifier having an input impedance of 100 megohms. Potential profiles were taken with shield in and out for two neutralizer conditions. The profile shown in figure 7 was obtained when the neutralizer was in a normal operating mode. The peak potential was about 8 and 4.5 V above ground with the shield in and out, respectively. With the shield in, the total potential difference between the neutralizer and the beam center was increased by virtue of the rise in beam floating potential and the decrease in neutralizer floating potential.

The profile obtained during poor beam neutralization caused by reducing neutralizer keeper current to off-normal values is shown in figure 8. The peak value of beam floating potential was three times higher than normal, and the difference between shield-in and shield-out potentials was much greater. The

effects of beam shield on beam potential were seen to be accentuated when neutralization was poor. In both instances, the presence of the shield appears to have broadened the potential profile, an effect also noticed with the ion beam current density profile.

The effect of floating or grounding the beam shield electrically is shown in figure 9. The neutralizer operated in the normal mode. No significant difference was observed in the beam region except that a grounded shield brought the potential profile closer to ground potential both at the positive peak and the negative wings.

Distribution Pattern of Fringe Ions

One of the spacecraft-thruster interfaces of concern is the distribution pattern of ion along the beam edge capable of sputter erosion. Current density profiles have been obtained, usually along a beam diameter, but a full two-dimensional pattern is of considerable interest. One method of obtaining a qualitative definition of the beam boundary is to sputter-erode a target of uniformly coated aluminum film. The relative amounts of erosion in different areas produced over a given length of time is indicative of current density. The size of erosion patterns obtained on targets at different axial distances permits an estimate of beam divergence. Finally, the ultimate size of a pattern after a long test could define the limiting radial distances at which sputter erosion occurs.

To correlate the target pattern with the ion source, a close-up view of the accelerator grid is shown in figure 10. Because the beam holes are located on the vertices of equilateral triangles, the smallest angle of symmetry is 30°. For ease of visulaization, the axes of symmetry were chosen to be 60° apart drawn from the grid center to the middle of seven holes in line along the side of a hexagon. The boundary of holes idealized with straight line segments is nevertheless complex, consisting of seven segments. This idealized boundary will be used to examine the erosion pattern sputtered on targets at two locations.

The erosion pattern obtained at a target distance of 50 cm after 11 hours of thruster operation is shown in figure 11 (back-lighted photograph). The central hole was 26 cm in diameter which passed approximately 50 mA of beam current integrated from the beam profile assuming axial symmetry. The collected target current measured when the aluminized surface was uniform was 23 mA. This value agrees closely with the difference between the total beam current of 72 mA and the integrated current passing through the central hole.

The darker rim around the central hole was the area exposed by the back cover sheet, hence subject to backsputter deposition from the facility walls. The lighter mid-region was completely clear on both sides of the mylar sheet, the front aluminized coating having been completely sputtered away and the back

side protected from backsputtered material. The variegated islands around the periphery were areas at various states of sputter erosion. Where beam density was high, the islands were almost clear. Other regions appeared as small isolated spots.

The degree of erosion along a radial line did not decrease motonically. It appears that some of the outer beamlets were sufficiently divergent to leave an unsputtered border between the mid-region and the islands. This interpretation is supported by the photograph in figure 10 which shows some of the outer beam holes notched on the outside edge, possibly by divergent ion. More recent examination of the accelerator grid has shown erosion on these outside edges, indicating persistent diverging of these beamlets. These divergent ions may also account for the broad wings in the otherwise peaked beam profile shown in figure 6.

The idealized beam hole boundary consisting seven line segments is drawn to an arbitrary scale in figure 11. To approximate the beam expansion boundary, it was assumed that each of the boundary holes is a point source of ions diverging at some conical half-angle, β. The most radially outward ray from a given beam hole will be located in a radial plane passing through the beam hole. The radius at which the ray interrupts a target located at distance, L, from the grid plane is $L \tan \beta + r$, where r is the radial location of the beam hole on the grid. Because $L \tan \beta$ is a constant for all edge beam holes, the expanded beam boundary on the target can be drawn point by point from the idealized beam hole boundary a constant radial distance along the radial line passing through each point. The expanded beam boundary for $\beta = 30^{\circ}$ is shown in figure 11. The sputter erosion pattern shows some correspondence to the expanded beam boundary and indicates a β angle between 30° and 35°. Less precise but simpler circular boundaries corresponding to assumed half angles of 30° and 35° from the thruster axis are also shown in figure 11. These angles when compared to the calculated angles shown in figure 6 indicate that sputtering ions may have existed beyond the resolution limit of the measured beam profile.

The erosion pattern obtained at a target distance of 97.8 cm after 78 hours of operation is shown in figure 12. Details around the central hole and the clear mid-region were similar to the 50 cm target of figure 11. Because of the distance and the long duration, the sputtered islands had coalesced. Some dark border regions between the completely sputtered mid-region and the outer rim remained as unsputtered aluminized coating. The two large isolated spots in the lower left corner of the target are believed to be mercury corrosion of the aluminum coating after exposure to atmosphere.

The erosion pattern was wider than the target material. Expanded beam boundaries corresponding to β angles of 30° and 35° have been superposed on the pattern. Also shown are the simplified circular boundaries. In both the

50 and 97.8 cm targets the boundary of erosion appears to be located at radii corresponding to angles between 35° and 40° from the thruster axis.

A horizontal cross-section schematic through the thruster and neutralizer axes is shown in figure 13. The beam shield, sputter targets, and a scaled plot of the beam profile measured in this plane are included. The erosion boundaries obtained on the targets are indicated with their respective diameters tabulated at their axial distances. On the beam shield side, a ray drawn from the outermost beam hole to the erosion boundaries appears to intercept the beam shield. It is also evident that this ray to the erosion boundaries pass through regions of the beam profile where current measurement did not have adequate resolution.

The cause of these erosion boundary anomalies are not clearly known. It is obvious that considerable operating time is required to sputter through the aluminized coating when the incident flux density is low. The tip of the beam shield intercepted a 28° angle ray from the outermost beam hole in the horizontal plane. The ion source was a two-dimensional source whereas the beam shield had a tuncated cylindrical profile with the peak height only in the horizontal plane. It is also possible that some bending of the ion trajectory occurs after passing the beam shield.

Contaminant Deposition

Photographs of the 24 contaminant deposition samples are shown in figure 14. To preserve the relative order of placement as laid out in figure 3, the slides from each bank are grouped in pairs of two glass and two quartz samples. Figure 14(a) shows glass slides, W11 and W12, alternated with quartz slides W1 and W2 on the left bank and their symmetrical counterparts on the right.

The irregular dark spot in the center of each glass slide was the cement used to fasten a mounting clip. The dark borders along the top of the glass slides were caused by backsputtered deposition on the back of the slide. To aid in the interpretation of the deposition pattern, the various regions marked with numbers on sample E12, for example, will be examined. Region 1 was masked in front and covered in the back by the support bracket, hence clear of any deposits. The relative amount of backsputtered material can be seen from region 2 which was masked on the front but exposed in the back. Conversely, region 3 was masked on the back and exposed in the front, thus showing only the front deposit.

Region 4 was exposed front and back, thus collecting backsputtered wall material on the back and thruster efflux on the front. Region 5 was covered on the back by the support bracket thus showing only the front deposit. A particular feature not found in other slides can be seen in slide E12. The left 1/4 of this slide was clear but the remaining length collected deposit. Efflux from the

thruster was arriving over the full length of the slide, but a competing process of sputtering by energetic ions occurred at a rate sufficient to cause no net deposition. This effect has been discussed in reference 2 and also observed experimentally in the investigation of reference 8. A more detailed analysis of this slide in subsequent paragraphs will quantify light transmittance as a function of position.

Other slides can be interpreted similarly. Slides E11 and W11 were free of deposits on the front because of sputtering. All other W slides were also deposit-free on the front because of the umbra of the beam shield. The dark border along the top of those slides at smaller angles from the thruster axis was backsputtered wall material. At larger angles, the amount of backsputtered deposits decreased because of the diminishing view factor presented to the rear tank wall. All enclosed slides, W1 to W6, were free of deposits because of the beam shield and enclosure shielding from the rear tank wall.

Varying amounts of front and back face deposits can be seen on the unenclosed slides, E11 to E16. The enclosed slides show a range of front face deposition only because they look radially into the thruster accelerator. No visible deposits existed on either slide E6 or W6 which were located in the back hemisphere. As noted in Apparatus and Procedure, the right bank was heated to about 20° C and the left bank reached equilibrium temperatures of the order of -30° C. From visual inspection, there was no apparent difference in deposit characteristics attributable to the difference in slide temperatures.

Deposition sample W12 was analyzed for total transmittance of light using a Joyce-Loeble Automatic Integrating Microdensitometer. This densitometer was a double-beam null-balance type with a measuring aperture size of 1/50 by 1/50 microns. The light source was a tungsten lamp with a detector similar in spectral response to a 1-P28 photomultiplier. The results of the density measurements converted to total transmittance relative to a known clear region of the sample is shown in figure 15. The circled numerals indicate the regions of the sample with various types of exposure to the vacuum facility environment. The densitometer scans were made along the broken lines marked AA and BB. The resulting transmittance profiles are labeled A and B, respectively, as a function of angle from the thruster axis. Because it is relative to clear glass, the transmittance value is for the deposit itself. A later analysis will show the spectral transmittance of the glass itself.

The region near the vertical axis X-X is of special interest. As discussed previously, the left end of this slide was free of deposit because of the scrubbing action on the front and the mounting bracket on the back. The transmittance along A-A was indeed 100 percent here. The angular position of axis X-X where transmittance decreased was about 39°. The sputter target of figure 11 also shows that the boundary of erosion was slightly less than 40°.

The front-masked region 1 also had 100 percent transmittance. The A-A and B-B scans should be equal at angular positions from about 44° to 45° because of identical exposure conditions, namely front face only. Their transmittance agreed to within 4 percent. The transmittance profile of the deposit on quartz sample E2 is shown in figure 16. As expected, transmittance was essentially 100 percent except at the deposit where it was 80 percent as seen previously on glass slide E12. The size of the deposit was 0.5 by 1.3 cm. The aperture of the slide enclosure was 0.6 by 1.25 cm, thus indicating that the trajectories of deposited efflux were essentially parallel.

The total transmittance profile of sample E16 is shown in figure 17. Located at 90° from the thruster axis, the slide was subject to backsputtered deposition on both the front and back surfaces. The plane of the slide was essentially parallel to the thruster axis, but because the backsputter source at the rear tank wall was large, a finite view factor existed between it and the slide faces. The view factor was further modified by the shadowing effect of the adjacent slide enclosure.

Scan A-A showed that a small amount of deposition occurred on the front face in the back hemisphere, thus reducing transmittance by almost 10 percent. Analysis of enclosed quartz slides E5 and E6, not shown here, showed no visible deposit and 100 percent transmittance which tends to confirm that the deposit on slide E16 was backsputtered wall material.

Scan B-B showed almost the same transmittance profile as A-A. The absence of any change in region 3 which was masked on the back surface, also shows that the deposits were on the front face only.

The transmittance profile of sample W16 is shown in figure 18. Both scans yielded practically identical results. The deposits were clearly on the front face only and adjacent enclosed quartz slides, W5 and W6, showed 100 percent transmittance.

The spectral transmittance of quartz and glass slides were obtained with a Cary Model 14 Recording Spectrophotometer. Analyses were made over a wavelength band of 3300 to 12 000 Å which is the range of interest for silicon solar cells.

The transmittance profiles for several slides are shown in figure 19. The broken lines are for clean quartz and glass slides. The nominal transmittance of these slides are 92 percent because of an approximately 4 percent loss per face due to reflection and refraction. The transmittance loss of ultraviolet in glass was clearly evident below 4000 Å, whereas the loss in quartz was negligible.

Because of the relative complexity of spectral analysis, only selected sites of interest were examined in samples E2 and E12 for this preliminary presentation. As indicated in figures 15 and 16, E12-region 5 was a front face deposit at about 40.5° from the thruster axis. Region 5 of slide E2 was located at about 48°.

Both transmittance profiles were nearly identical at the longer wavelengths. All profiles were referenced to 100 percent transmittance so that the loss due to the efflux deposit is the difference between the clean slide and the sample. As expected, the deposits on both slides caused about the same amount of loss because of their similar density and composition. The deposits caused increasingly larger losses at shorter wavelengths. Below about 3750 Å, the loss due to the deposit on glass was difficult to assess because of the filtering effect of the glass itself.

CONCLUSIONS

An 8-cm engineering model mercury ion thruster fitted with a movable beam shield was tested in conjunction with various efflux diagnostic measurements. The beam shield had little effect on thruster operation. Moving the beam shield into position during thruster operation increased the accelerator drain current 10 percent and increased the neutralizer floating potential 1.5 V negatively with respect to facility ground. Ion beam floating potential increased about 3.5 V at the beam centerline with normal neutralizer operation.

The boundaries of energetic beam ions mapped by sputtering a 150 Å aluminum film showed peripheral irregularities and the presence of energetic ions at angles up to almost 40° from the thruster axis.

Unenclosed glass slides were used to monitor deposits of sputtered efflux from the thruster. Enclosed slides were free of backsputtered material and also clearly showed the effectiveness of the beam shield against sputtered metal efflux. The absence of deposits on enclosed slides at angles of 85° and greater, even on the side not protected by the beam shield, indicated no metal efflux in those regions.

REFERENCES

1. "8-cm Mercury Ion Thruster Subsystem Users Manual," TRW Defense and Space Systems Group, July 1977.

2. Zafran, S., editor, "Ion Engine Auxiliary Propulsion Applications and Integration Study," TRW, Redondo Beam, Calif., TRW-29999-6013-RU-00, July 1977, (NASA CR-135312).

3. Power, J. L., "Planned Flight Test and Interface Measurements with a Small Mercury Ion Thruster (Part I)," AIAA Paper 78-647, Apr. 1978.

4. Herron, B. G., Hyman, J., Hooper, D. J., Williamson, W. S., and Collett, C. R., "Engineering Model 8-cm Thruster System," AIAA Paper 78-646, Apr. 1978.

5. Hyman, J., Jr., Dulgeroff, C. R., Kami, S., and Williamson, W. S., "One-Millipound Mercury Ion Thruster," AIAA Paper 75-386, Mar. 1975.

6. Williamson, W. S., "Dispersion Properties of Engineering Model 8-cm Thrusters," AIAA Paper 78-648, Apr. 1978.

7. Banks, B. A., et al., "8-cm Mercury Ion Thruster System Technology," AIAA Paper 74-1116, Oct. 1974.

8. Weigand, A. J., and Mirtich, M. J., "Measurement of Sputtered Efflux from 5-, 8-, and 20-cm Diameter Mercury Ion Thrusters," AIAA Paper 75-358, Mar. 1975.

ORIGINAL PAGE IS
OF POOR QUALITY

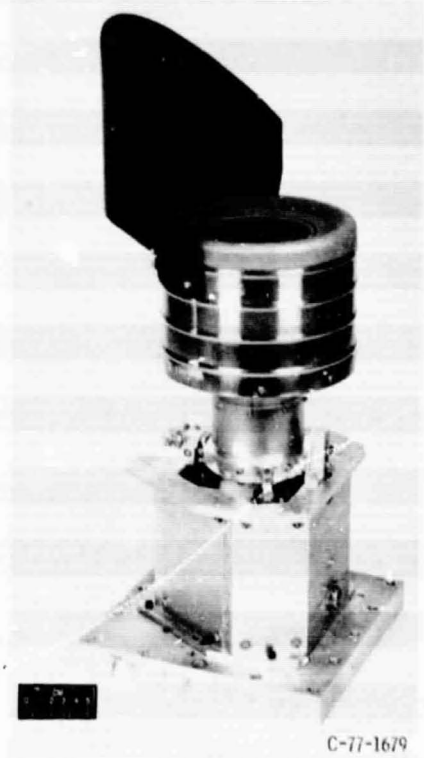

Figure 1. - 8-Cm EM thruster with gimbal mount and beam shield.

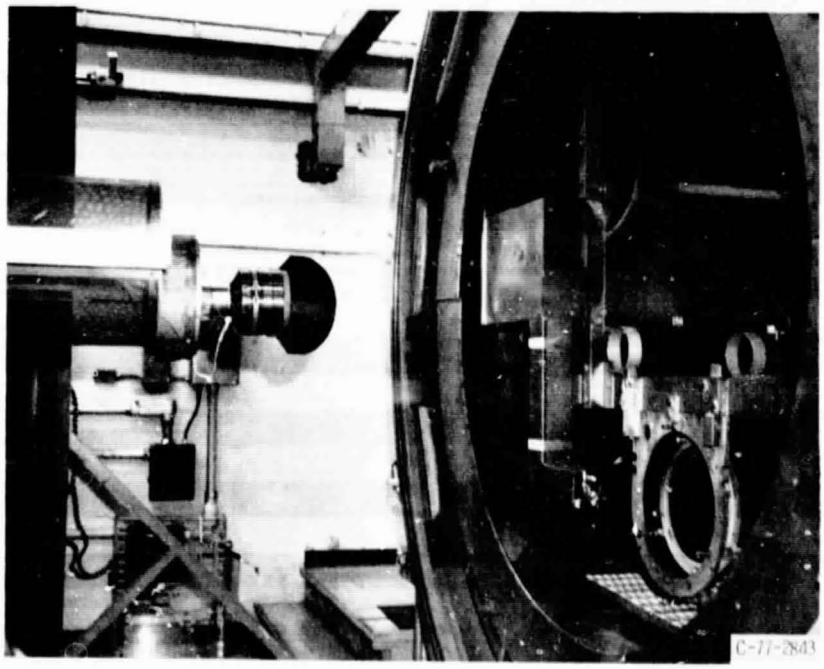

Figure 2. - 8-Cm thruster and test facility.

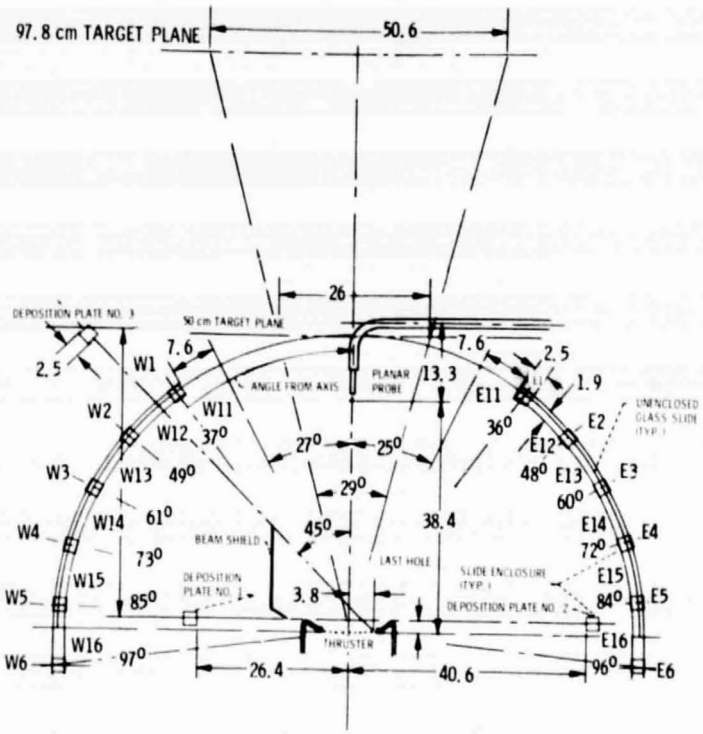

Figure 3. - Schematic layout of efflux diagnostics instrumentation. All dimensions in centimeters.

ORIGINAL PAGE IS
OF POOR QUALITY

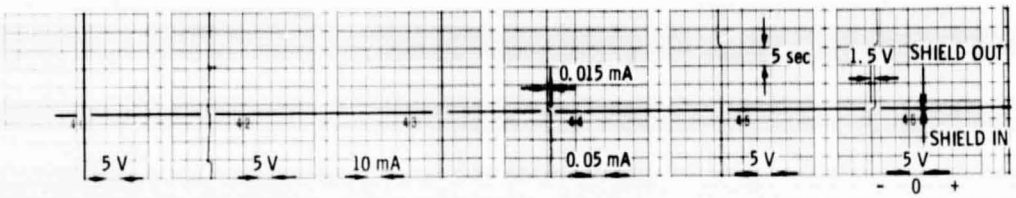

(a) SHIELD-IN TO SHIELD-OUT TRANSIENT.

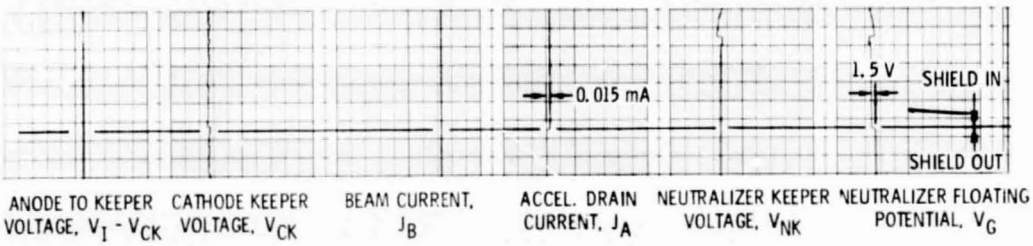

(b) SHIELD-OUT TO SHIELD-IN TRANSIENT.

Figure 4. - Transient record of thruster operation during beam shield movement.

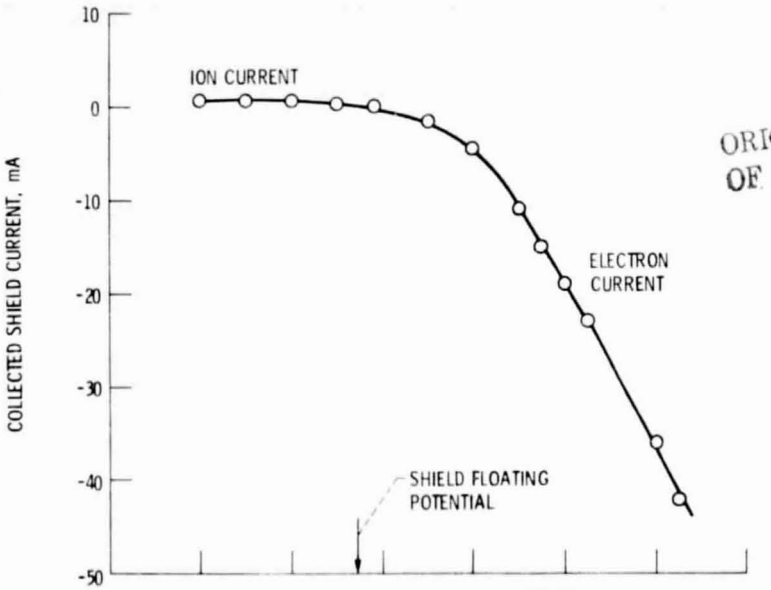

(a) CURRENT FROM SHIELD TO GROUND.

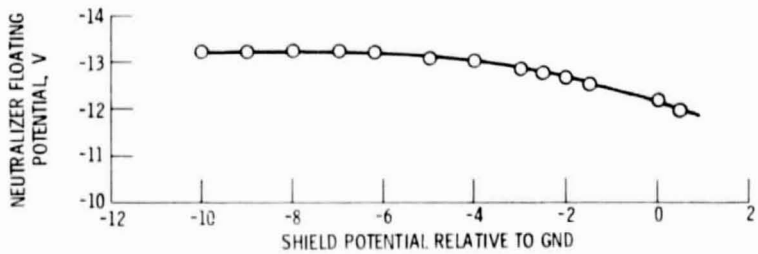

(b) NEUTRALIZER FLOATING POTENTIAL.

Figure 5. - Effects of shield bias on shield current and neutralizer floating potential.

ORIGINAL PAGE
OF POOR QUALITY

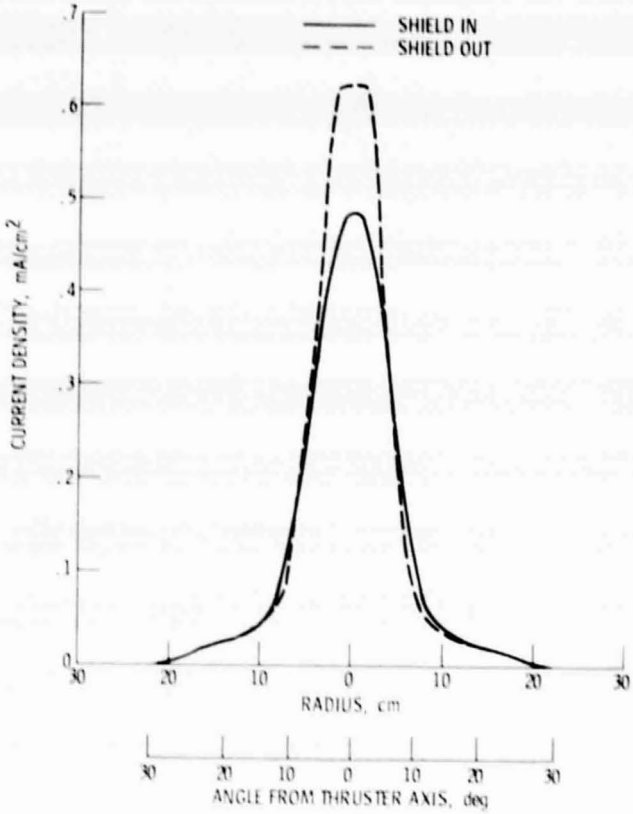

Figure 6. - Ion beam current density profiles.

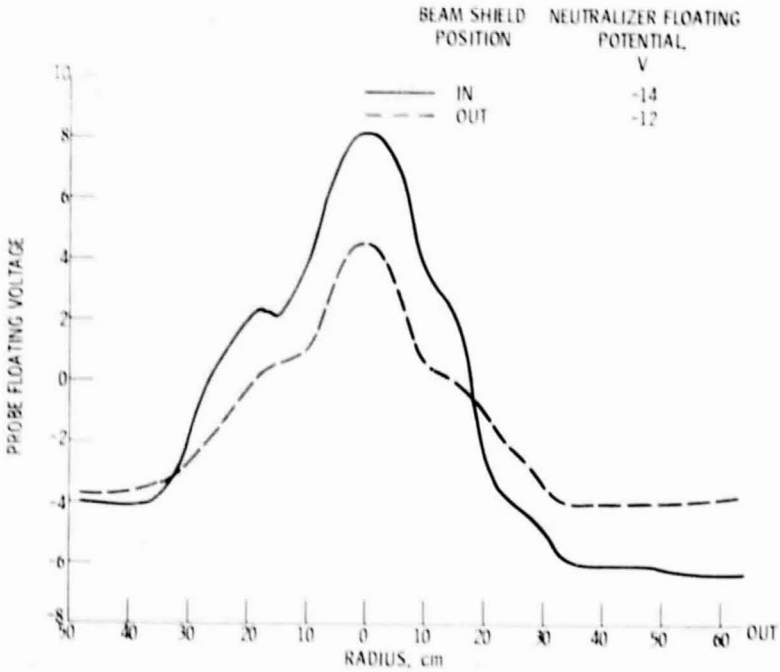

Figure 7. - Ion beam floating potential profile with a floating beam shield in and out of position. Normal neutralizer operation. Neutralizer keeper current, 0.5 A.

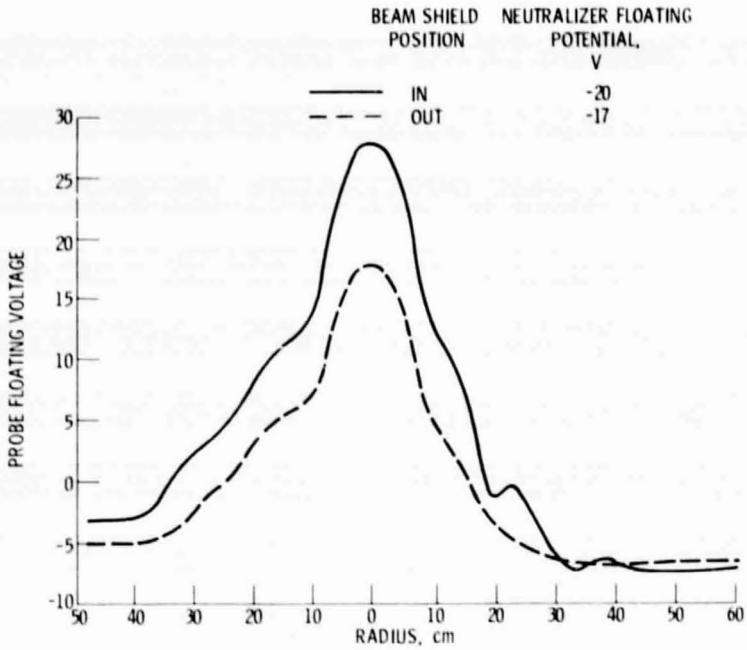

Figure 8. - Ion beam floating potential profile with a floating beam shield in andout of position. Off normal operation. Neutralizer keeper current, 0.33 A.

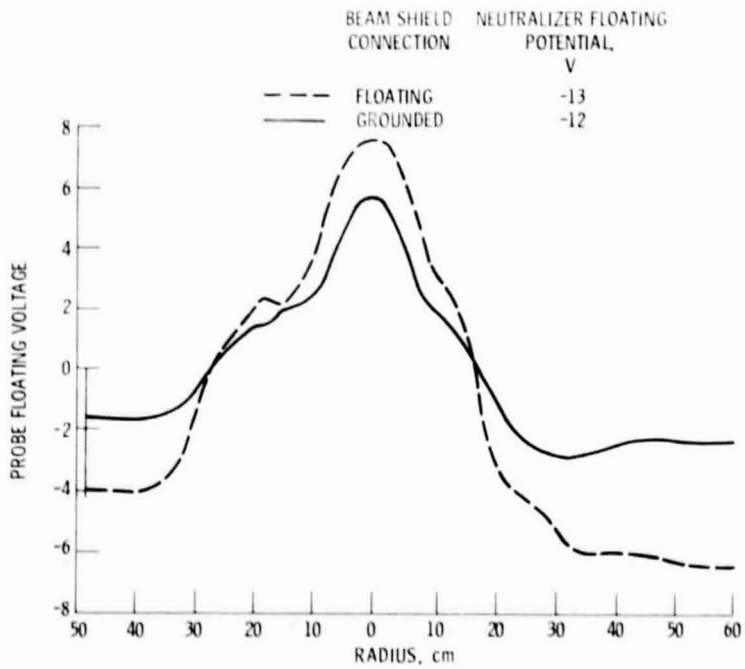

Figure 9. - Ion beam floating potential profile with beam shield floated and grounded. Neutralizer keeper current, 0.5 A.

ORIGINAL PAGE IS
OF POOR QUALITY

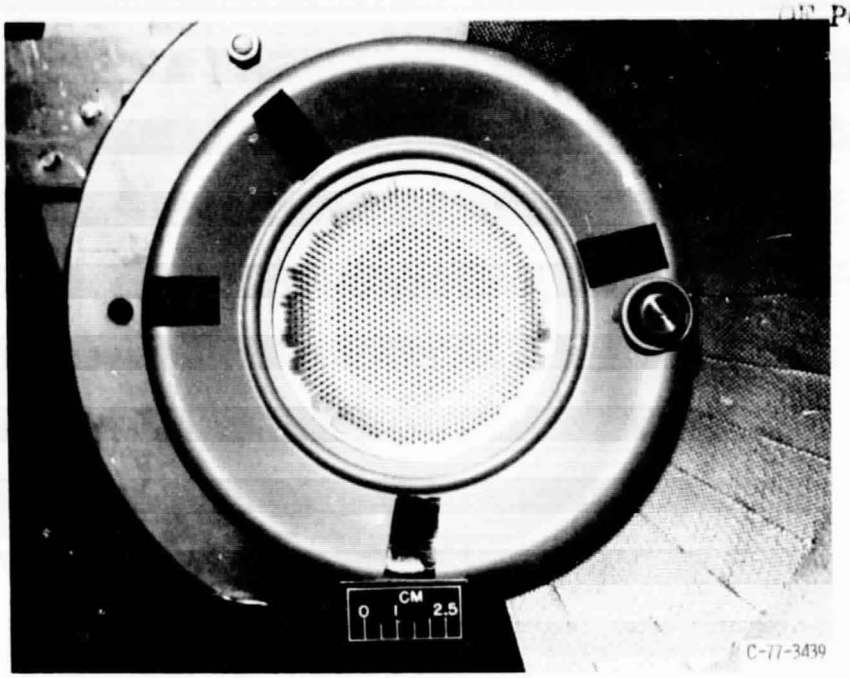

Figure 10. - Close-up view of accelerator grid.

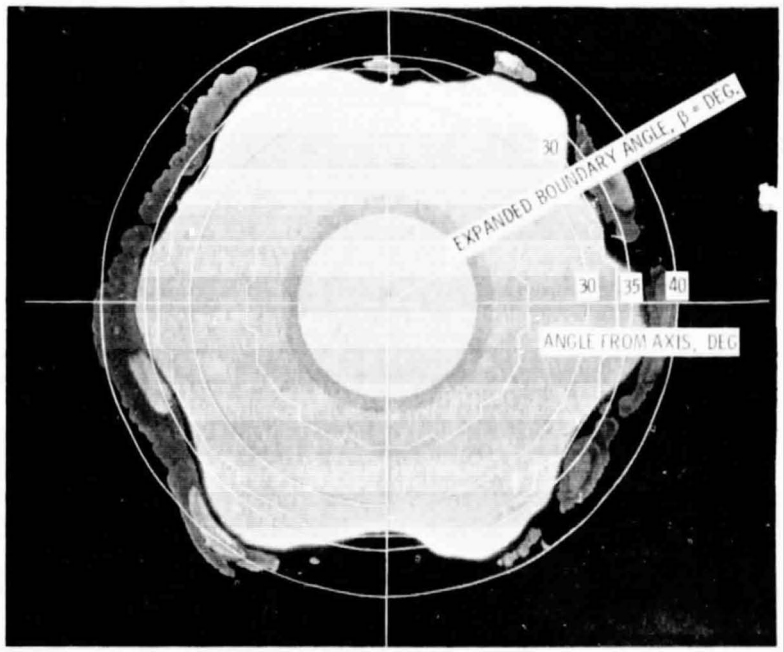

Figure 11. - Erosion pattern on target at 50 cm distance.

ORIGINAL PAGE IS
OF POOR QUALITY

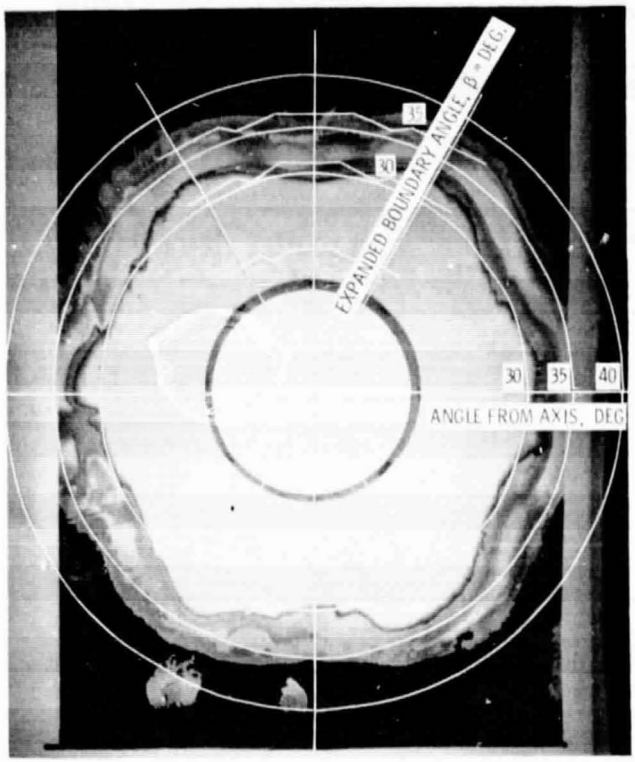

Figure 12. - Erosion pattern on target at 97.8 cm distance.

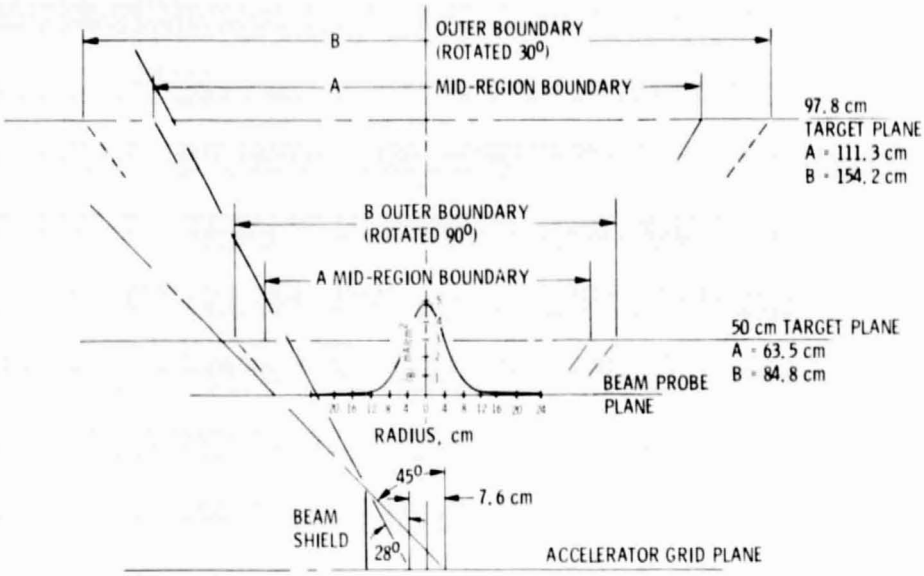

Figure 13. - Horizontal section scehmatic of thruster and targets.

ORIGINAL PAGE IS
OF POOR QUALITY

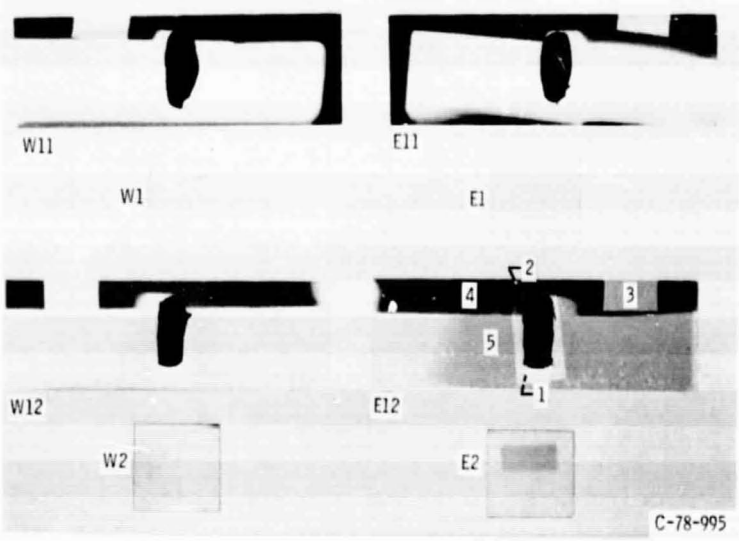

(a) DEPOSITION SAMPLES LOCATED BETWEEN 25 AND 49 DEGREES FROM THRUSTER AXIS.

Figure 14. - Efflux deposition samples.

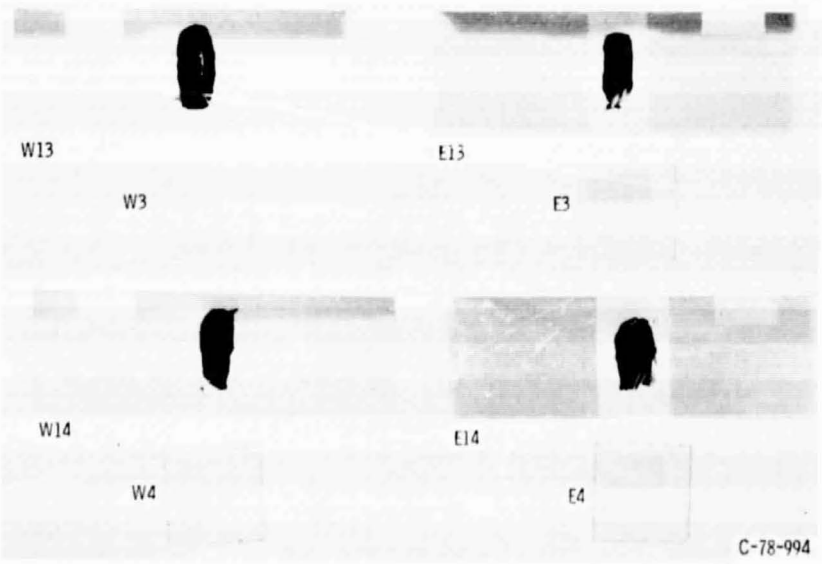

(b) DEPOSITION SAMPLES LOCATED BETWEEN 49 AND 73 DEGREES.

Figure 14. - Continued.

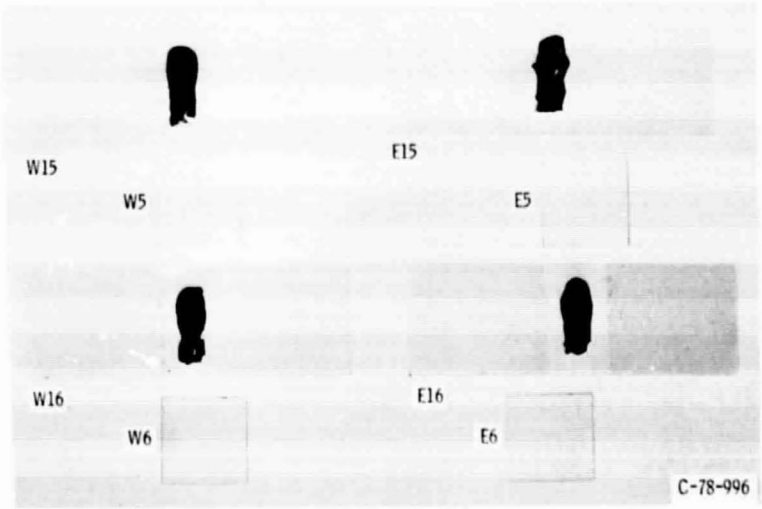

(c) DEPOSITION SAMPLES LOCATED BETWEEN 73 AND 97 DEGREES.

Figure 14. - Concluded.

ORIGINAL PAGE IS
OF POOR QUALITY

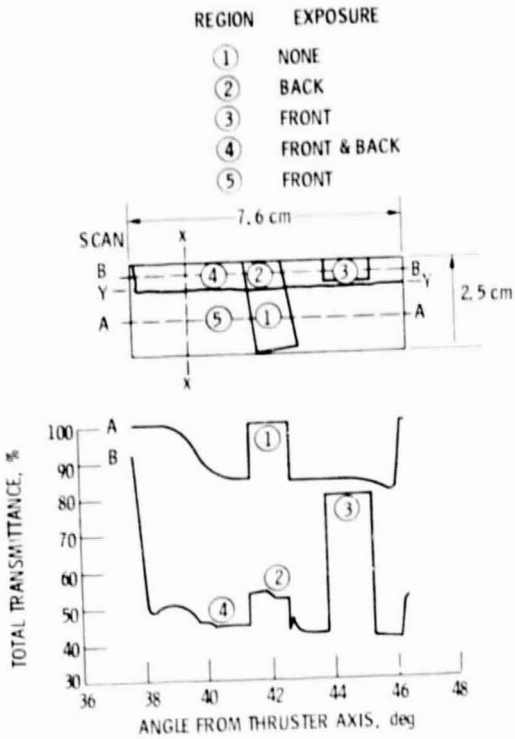

Figure 15. - Total transmittance profile of deposition sample E12.

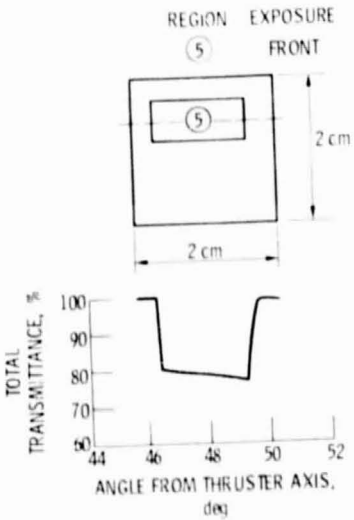

Figure 16. - Total transmittance profile of deposition sample E2.

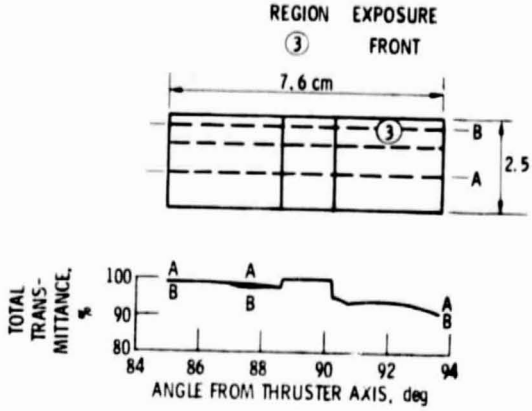

ORIGINAL PAGE IS OF POOR QUALITY

Figure 17. - Total transmittance profile of deposition sample E16.

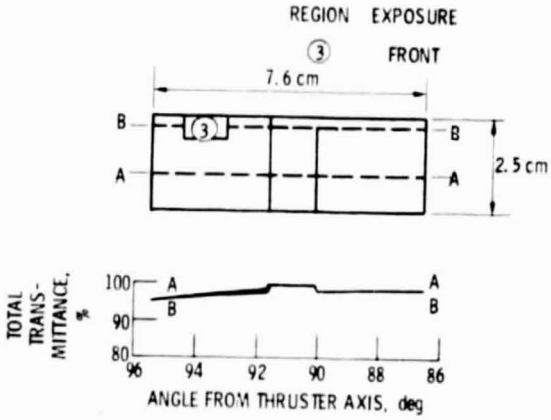

Figure 18. - Total transmittance profile of deposition sample W16.

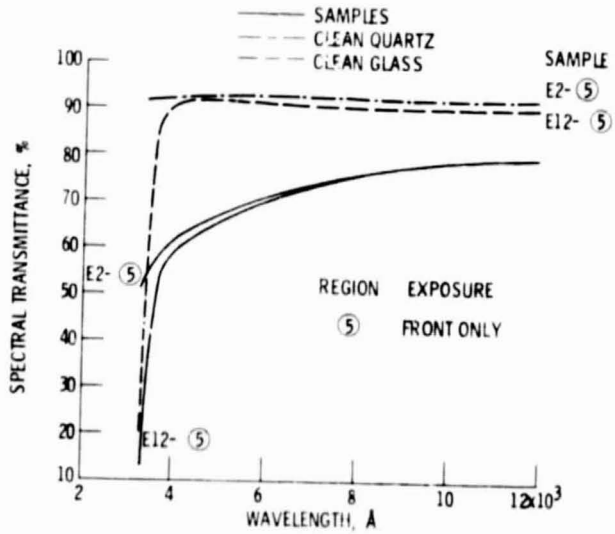

Figure 19. - Spectral transmittance of deposition samples.